



Lift Disturbance Cancellation with Rapid-Flap Actuation

Albert Medina*

Air Force Research Laboratory, Wright-Patterson Air Force Base, Ohio 45433

and

Maziar S. Hemati†

University of Minnesota, Minneapolis, Minnesota 55455

<https://doi.org/10.2514/1.J059865>

Mitigation of vertical aerodynamic disturbances by means of a simple mechanical flap is investigated experimentally. A wall-to-wall NACA 0006 wing is bisected about the midchord for a 50%-chord flap length. Experiments are performed in a water tunnel at a chord-based Reynolds number of $Re = 4 \times 10^4$. The wing is driven in a sinusoidal vertical plunge motion as a spatially uniform, temporally varying surrogate to a vertical disturbance. Concurrently, the flap is actively deflected in a survey of kinematic parameters designed to suppress the influence of a plunge-induced disturbance. Plunge rates explored amount to disturbances incurred over a temporal range from one convective time to eight convective times. Two methodologies are employed to guide selection of flap deflection phase and amplitude necessary to preserve the baseline zero-lift state ($\alpha = 0^\circ$) of the undisturbed wing. In the first method, Theodorsen's model is applied to arrive at an analytical solution to flap kinematics for a given prescribed plunge history. The theoretical derivation makes the standard assumptions of attached flow, planar wake, and no leading-edge vortical formations. Direct force measurements reveal reduction in lift transients by flap actuation of up to 87%, verifying the applicability of Theodorsen's classical model. Further improvement is sought in a second method where empirical state-space modeling is formulated for lift cancellation. In this approach two separate lift models for wing plunge and flap deflection are constructed independently, and their superposition is employed to approximate the total lift in combined plunge and deflection motions. It is shown that although the empirical state-space approach performs similar to the inviscid theory of Theodorsen's model, the empirical model proves more effective in suppressing the formation of the leading-edge vortex induced by plunge.

Nomenclature

a	=	smoothing parameter
b	=	semichord length
C_L	=	lift coefficient
C_k	=	Theodorsen function
c	=	chord length
h	=	plunge position
k	=	reduced frequency
\mathcal{L}	=	Laplace transform
L	=	lift
Re	=	Reynolds number, cU_∞/ν
U_∞	=	freestream speed
\tilde{x}	=	internal state of the system
y	=	state-space model output
α_{eff}	=	effective angle of attack
α_{LE}	=	leading-element angle of attack
δ	=	flap deflection angle
θ	=	state-space model input
\hat{k}	=	motion rate
σ	=	fitting parameter
ϕ	=	flap-deflection phase lead

I. Introduction

ATMOSPHERIC disturbances present considerable challenges to airborne systems. This is of particular consequence to small unmanned aerial vehicles owing to the relatively light weight and

small form factor of the craft in predominantly low-altitude operation. Such altitudes introduce transient velocities characteristic of the atmospheric boundary layer, resulting in temporal loading histories of the lifting surfaces that are often difficult to predict. Nevertheless, mitigation strategies would seek to preserve the prescribed flight path and maintain control authority in the presence of flowfield disturbances. Though disturbances may be highly three-dimensional in nature, fundamental works have examined the effects of orthogonal velocity components in isolation such as streamwise oscillations [1–5] and transverse encounters [6–10]. Although streamwise velocity surges are cause for significant deviation in dimensional loading, normalization by instantaneous relative freestream velocity offers some reconciliation among loading profiles [4,11]. Further, in combined pitching and surging experiments by Mueller-Vahl et al. it was demonstrated that full boundary-layer separation was determined by the instantaneous Reynolds number near maximum pitch incidence [11]. A predominant effect of transverse velocity fluctuations is the imposition of an effective angle of attack. Depending on the relative magnitude of the vertical flow speed the effective angle of attack may induce flow separation, potentially resulting in dynamic stall and/or trailing-edge vortical formations.

Recent parametric studies on the rapid transient motion of a conventional flap have documented an immediate lift response in some proportion to the flap deflection rate [12–14]. Such a response was not reserved to attached flows on a wing but also extended to massively separated flows where the extent of flow entrainment near the wing trailing edge was shown to have dependence on the direction of the deflection [14]. A simplified analytic model for lift coefficient history, composed of 1) added mass [15], 2) pitch rate or virtual camber, and 3) quasi-steady lift from airfoil theory, was moderately successful for transient lift response, but ignored wake effects. Such wake effects can be recovered to the extent that the planar wake assumption is valid for sinusoidal motions using Theodorsen's formula for a flapped airfoil (see, e.g., Jaworski's presentation in [16]). In experiments of a 50%-chord flap aboard a NACA 0006 wing it was found that as the rate of flap deflection increased, the inviscid solution for lift was recovered, or alternatively the penalty of flow separation was attenuated [13,17]. Indeed, at sufficiently high rates, often comparable to motions completed within one convective time, there

Presented as Paper 2018-3090 at the 2018 Fluid Dynamics Conference, Atlanta, GA, June 25–29, 2018; received 28 June 2020; revision received 2 April 2021; accepted for publication 6 June 2021; published online 16 August 2021. This material is declared a work of the U.S. Government and is not subject to copyright protection in the United States. All requests for copying and permission to reprint should be submitted to CCC at www.copyright.com; employ the eISSN 1533-385X to initiate your request. See also AIAA Rights and Permissions www.aiaa.org/randp.

*Research Scientist, Aerodynamic Technology Branch, Aerospace Systems Directorate. Senior Member AIAA.

†Assistant Professor, Department of Aerospace Engineering and Mechanics, Twin Cities. Senior Member AIAA.

was a significant entrainment effect over the suction surface of the fore-element and trailing flap such that the mean of the lift hysteresis loop was well above both the corresponding measured static value. In extensions of the Goman–Khrabrov model to a flapped NACA 0006 wing, Medina et al. [17] proposed that the mean-lift offset be modeled following a parameter-varying model [18] with dependence on flap deflection rate and initial deflection angle.

Given the applicability of inexpensive modeling and the apparent speed of lift response to actuation, the traditional mechanical flap bears revisiting in the scope of disturbance mitigation. Fundamentally, this effort is largely rooted in separation control. However, realizing real-time feedback control with any given control method would necessitate a flow response with minimal delay, where it is unacceptable to endure a lag of several convective times between control initiation and aerodynamic response [19]. To this end, experiments on mechanical flap actuation by Rennie and Jumper [12] examined slower flap responses (in the context of the present work) and found no apparent lag in lift response. Further, it was shown that the deleterious effects of flow separation, which were measured in a static survey of flap incidence, were attenuated during dynamic flap deflection [20]. This is in contrast to the usual case for pointwise (fluidic or electric) flow control, where for several convective times upon actuator initiation, there is a dead-band in response or a negative response in lift [21]. In experiments by Sedky et al. [22] a transverse gust encounter by a cruising wing was marked with significant lift deviation. Through kinematic programming the wing was able to employ a pitch maneuver to regulate lift for significant reduction in transient force. Such a transverse gust, introduced as a sine-squared velocity profile, represents a disturbance incurred over two chord lengths of travel, and it is of negligible influence once the wing exits the vertical field and recovers [6,22]. The relatively short duration of spurious gusts and the speed of the associated recovery introduce considerable time constraints for real-time flow control and highlight the need for control mechanisms potentially delivering expanded bandwidths. Be it pointwise, control surface, or kinematic-based control, the underlying goal of most disturbance-mitigation methods is the notional rejection of flow separation.

In the present work, Theodorsen’s model is again used for a NACA 0006 wing hinged at the midchord. The fore element is held fixed at zero incidence ($\alpha = 0^\circ$) and the 50%-chord flap is engaged in oscillatory pivot about the zero-incidence angle at the hinge. Thus the mean lift performance amounts to zero, regardless of flap deflection rate or amplitude. A spatially uniform, temporally varying disturbance is introduced by imposing a sinusoidal-plunge motion on the entire wing (fore-element and flap in unison). At sufficiently high plunge rates the effective angle of attack, as calculated at the wing leading edge, may exceed static attached angles causing the separation and vortical roll-up about the leading and trailing edges. The flap is driven harmonically at the same frequency as the plunge motion in an attempt to cancel, or at the very least mitigate, the excursion in lift incurred in plunge from an otherwise zero-lift state. In this study a parameter sweep of the disturbance frequency and amplitude is investigated, and the lift cancellation is informed by both

Theodorsen’s formula and an empirical state-space model. In recourse to Theodorsen’s model the method of McGowan et al. [23] is employed to seek lift equivalence between the plunge and flap deflection motion contributions to lift. The aim is to find at least an approximately suitable model for the plant (aerodynamic response of the flap) and the disturbance (the plunge), for what will eventually be a feed-forward control system, relying on negation of the flap model; this would follow the approach of Kerstens et al. [24]. This study considers only the deterministic motion of the flap. To this end, in addition to the inviscid modeling approach, two empirical state-space models are also devised for lift-contributions from plunge and flap deflection, respectively. These state-space models are superposed to arrive at an approximation for disturbance mitigation. Through dye visualization it is revealed that the state-space model provides for greater suppression of leading-edge vortex over the inviscid modeling of Theodorsen’s formulation.

This paper is organized as follows: The water tunnel facility, test article, and wing kinematics are introduced in Sec. II. The theoretical framework of Theodorsen’s model is presented in Sec. III.A, where a lift equivalence is sought between lift contributions from plunge motion and flap deflection. Here the kinematic parameters are also summarized. Section III.B reviews the methodology of extracting state-space models for both pure plunge and pure flap deflection. Results are discussed in Sec. IV, by first examining the plunge-flap equivalence of Theodorsen’s model in Sec. IV.A followed by the state-space approach in Sec. IV.B. Finally, conclusions are given in Sec. V. This work follows from a previous submission to the 2018 Fluid Dynamics Conference [25].

II. Experimental Setup

Experiments were performed in the U.S. Air Force Research Laboratory (AFRL) Horizontal Free-Surface Water Tunnel, depicted in Fig. 1 (left). The tunnel has a 4:1 contraction and 46-cm-wide-by-61-cm-high test section with a freestream speed range of 3–105 cm/s and a streamwise turbulence intensity of $\sim 1.0\%$ for speeds between 7 and 80 cm/s. The tunnel is fitted with a three-degree-of-freedom motion stage, consisting of a triplet of H2 W Technologies linear motors, driven by AMC DigiFlex servo drives interfaced with a Galil DMC 4040 four-axis motion controller with user-selected proportional-integral-derivative gain constants for each axis. A plastic 3-D printed NACA 0006 airfoil of 20 cm chord (physical aspect ratio of 2.25), strengthened by spanwise carbon-fiber rods, is bisected about the midchord position as illustrated in Fig. 1 (right). The test article spans the test section with a nominal 1 mm gap at each wingtip. The fore element is rigidly connected to the plunge rod of the upstream vertical linear motor. The resulting aft element, or flap, is analogously connected to the downstream vertical linear motor, but it is constrained by a linkage mechanism to the fore element such that the relative motion between the two vertical motors results in a pitching motion of the flap. The gap between the two elements measures 0.5 mm and is bridged with a flexible rubber film of 0.2 mm thickness to prevent flare-up. The rubber film was constructed of pure Tango-Black, which provides high elasticity with a hardness of 61 Shore A

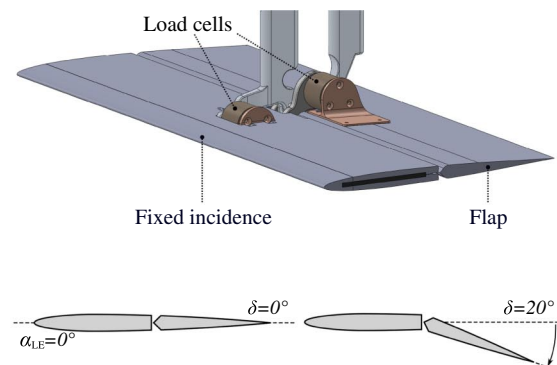
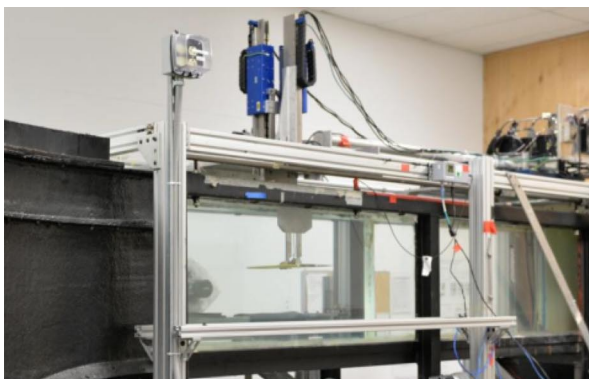


Fig. 1 Water tunnel facility (left). NACA0006 configuration and angular definitions (right).

Scale. Importantly, the flap was of no measureable consequence to resultant forces, as determined from direct comparisons with and without the film installed. The flap incidence angle is limited to $\pm 45^\circ$ with respect to the horizontal plane. The fore element fixed-incidence angle is $\alpha_{LE} = 0^\circ$, corresponding to an attached flow with zero net lift. Experiments are performed at Reynolds number $Re = 40$ k.

Force measurement was conducted via two ATI NANO-25 IP68 six-component force balances. Each airfoil element was supplied a dedicated force balance affixed to its respective frame. Importantly, there is no mechanical connection between the fore and aft elements; the forces measured for each element were therefore measured independently. Measurements were sampled at a rate of 1 kHz and treated by a second-order Butterworth low-pass filter with a cutoff frequency of 8 Hz. For periodic motions, the flap motion and the wing-plunge continue for 70 periods. The first few periods evince effects of startup transients; therefore the first 10 periods are discarded for the purpose of phase averaging. Likewise, the last 10 periods are also discarded. Force histories were constructed from phase averaging over the remaining 50 consecutive periods of motion. Static forces were derived from time averaging over a hold period of 10 s for each flap deflection angle. Lift coefficient was nondimensionalized as $C_L = (L/0.5\rho U_\infty^2 S)$, where L is the measured lift, ρ is the fluid density, U_∞ is the freestream speed, and S is the planform area.

Planar flow visualization was performed at the three-quarter spanwise position. Rhodamine-590 was introduced at the leading edge and the trailing edge of the airfoil and fluoresced by an Nd:YLF laser sheet (Photonics Industries DM50-527, 55 mJ/pulse, 10 kHz max). To minimize surface reflections the camera was outfitted with an optical filter (Tiffen, Orange 21) compatible with the fluorescence emission.

The kinematic schedules of airfoil plunge $h(t)$ and flap deflection $\delta(t)$ are, respectively, expressed in Eq. (1):

$$h = h_0 e^{i\omega t} \quad \delta = \delta_0 e^{i(\omega t + \phi)} \quad (1)$$

where ω is the angular frequency, h is the wing plunge history, and h_0 is the plunge amplitude. Analogously, the flap deflection motion was a sinusoid of amplitude δ_0 and with a phase lead angle of ϕ over the plunge cycle. The plunge motion was employed as a kinematic-driven disturbance that provided a spatially uniform, temporally varying vertical velocity component. It is important to note that the sinusoidal vertical velocity variation of the airfoil is not equivalent to a vertical variation of the fluid domain. That is, the apparent mass contributions from the acceleration of motion differ between the two. The lift coefficient was approximated as the summation of airfoil plunge and flap deflection contributions given by Eq. (2) as

$$C_L = C_{L,\text{plunge}} + C_{L,\text{defl.}} \quad (2)$$

where the subscripts denote the respective contributions of airfoil plunge and flap deflection to lift coefficient. Note the exclusion of a steady-state incidence term in Eq. (2), as the baseline situation (no plunge and no flap deflection) has zero lift.

III. Theory

A. Theodorsen Modeling

Following Jaworski's treatment of Theodorsen's model [16] the respective lift contributions of airfoil plunge and flap deflection may be expressed as

$$L_{\text{plunge}} = \pi \rho b^2 \ddot{h} + 2\pi \rho U_\infty b C_k \dot{h} \quad (3)$$

and

$$L_{\text{defl.}} = \pi \rho b^2 \left[\frac{1}{2} U_\infty \dot{\delta} + \frac{2}{3\pi} b \ddot{\delta} \right] + 2\pi \rho U_\infty b C_k \left[\frac{2+\pi}{2\pi} U_\infty \dot{\delta} + \frac{4+\pi}{4\pi} b \ddot{\delta} \right] \quad (4)$$

where ρ is the fluid density, b is the semichord length ($c/2$), U_∞ is the freestream speed, and C_k is the Theodorsen function ($C_k = F(k) + iG(k)$) for reduced frequency $k = \omega b/U_\infty$. Equations (3) and (4) were derived using a small-angle approximation, assumed a planar wake, and were formulated for an attached flow.

Following McGowan et al. [23], cancellation of lift from airfoil plunge by lift from flap deflection is achieved by setting Eq. (2) to zero:

$$L_{\text{plunge}} = -L_{\text{defl.}} \quad (5)$$

Although the lift response is modeled separately for plunge and deflection, a key assumption is that the linear superposition of the two components is valid. To derive an analytical expression for flap deflection amplitude and phase necessary for the cancellation of plunge effects, the kinematic schedules of Eq. (1) for h and δ and their respective derivatives are substituted into Eqs. (3) and (4). The resulting complex lift coefficient expressions are then substituted into the zero-lift criterion of Eq (5), where the real portion of the final expression yields Eq. (6):

$$\begin{aligned} & \left[\underbrace{\pi \rho b^2 \omega^2 + 2\pi \rho U_\infty b G \omega}_{A_1} \right] h_0 \\ &= \left[\underbrace{[-(\pi/2)\rho b^2 U_\infty - (2+\pi)\rho U_\infty b G - (4+\pi/2)\rho U_\infty b^2 \omega F]}_{A_2} \sin \phi \right. \\ & \left. + \underbrace{[-(2/3)\rho b^3 \omega^2 + (2+\pi)\rho U_\infty^2 b F - (4+\pi/2)\rho U_\infty b^2 \omega G]}_{A_3} \cos \phi \right] \delta_0 \end{aligned} \quad (6)$$

And the imaginary portion yields Eq. (7):

$$\begin{aligned} & \left[\underbrace{-2\pi \rho U_\infty b \omega F}_{B_1} \right] h_0 \\ &= \left[\underbrace{[-(2/3)\rho b^3 \omega^2 + (2+\pi)\rho U_\infty^2 b F - (4+\pi/2)\rho U_\infty b^2 \omega G]}_{B_2} \sin \phi \right. \\ & \left. + \underbrace{[(\pi/2)\rho U_\infty b^2 \omega + (2+\pi)\rho U_\infty^2 b G + (4+\pi/2)\rho U_\infty b^2 \omega F]}_{B_3} \cos \phi \right] \delta_0 \end{aligned} \quad (7)$$

Division of Eq. (6) by Eq. (7) eliminates the dependency on plunge and flap deflection amplitudes. Further division of the numerator and denominator by $\cos \phi$ produces an expression for flap-pitch phase lead:

$$\phi = \tan^{-1} \left(\frac{B_1 A_3 - A_1 B_3}{A_1 B_2 - B_1 A_2} \right) \quad (8)$$

The procedure undertaken in this work first prescribes a flap deflection amplitude and reduced frequency k . Then using Eq (8) the corresponding phase lead ϕ is calculated. The phase lead is then substituted into either Eq. (6) or Eq. (7) to determine the ratio of plunge amplitude to flap deflection amplitude, h_0/δ_0 . When these calculated kinematic parameters are executed in experiments the theoretical result is an identically zero lift coefficient history. The Theodorsen approach is employed in examining the plunge-disturbance mitigation capabilities of flap amplitudes of $\delta_0 = 10^\circ$ and 20° for reduced frequencies $k = [0.3989, 0.7979, 1.5959, 3.1919]$. Such operational frequencies invoke a highly unsteady flowfield and invite greater nonlinearity. Further, under the constraints of the kinematic approach presented above there exists a inverse relation between reduced frequency and plunge amplitude. The selected frequency

range approaches the mechanical limitations of the vertical linear motors driving the test article. Cases to be examined within the theoretical framework of Theodorsen's model are summarized in Table 1 and plotted in Fig. 2.

B. Empirical State-Space Modeling

In this section, the approach used to extract a state-space model from an empirical sequence of input–output data is detailed. Similar empirical modeling approaches have been considered in [18,26,27]. This model was pursued in an attempt to improve upon the results of the theoretical Theodorsen model. The model input is denoted as $\ddot{\theta}$, which corresponded to $\ddot{\delta}$ for flap modeling and \ddot{h} for plunge modeling. The output for each model was the lift coefficient minus the lift at the initial set point $y = C_L - C_{L_0}$.

Specifically, a system of the form

$$\begin{bmatrix} \tilde{x}_{k+1} \\ \theta_{k+1} \\ \dot{\theta}_{k+1} \end{bmatrix} = \begin{bmatrix} \tilde{A} & B_\theta & B_{\dot{\theta}} \\ 0 & 1 & \Delta t \\ 0 & 0 & 1 \end{bmatrix} \begin{bmatrix} \tilde{x}_k \\ \theta_k \\ \dot{\theta}_k \end{bmatrix} + \begin{bmatrix} B_{\ddot{\theta}} \\ \Delta t^2/2 \\ \Delta t \end{bmatrix} \ddot{\theta}_k \quad (9a)$$

Table 1 Theodorsen model motion parameters

Case	Motion	h_0/b	ϕ , deg	$\delta(0)$, deg
Case 1: $k = 0.3989$, $\delta_0 = 10^\circ$	Flap+plunge	-0.3791	81.41	1.42
	Pure flap	0	180	-10
	Pure plunge	-0.3791	0	0
Case 2: $k = 0.7979$, $\delta_0 = 10^\circ$	Flap+plunge	-0.1985	77.99	2.08
	Pure flap	0	180	-10
	Pure plunge	-0.1985	0	0
Case 3: $k = 1.5959$, $\delta_0 = 10^\circ$	Flap+plunge	-0.1028	69.52	3.49
	Pure flap	0	180	-10
	Pure plunge	-0.1028	0	0
Case 4: $k = 3.1919$, $\delta_0 = 10^\circ$	Flap+plunge	-0.0596	52.45	6.09
	Pure flap	0	180	-10
	Pure plunge	-0.0596	0	0
Case 5: $k = 0.7979$, $\delta_0 = 20^\circ$	Flap+plunge	-0.3971	77.99	4.16
	Pure flap	0	180	-20
	Pure plunge	-0.3971	0	0
Case 6: $k = 1.5959$, $\delta_0 = 20^\circ$	Flap+plunge	-0.2057	69.52	6.99
	Pure flap	0	180	-20
	Pure plunge	-0.2057	0	0

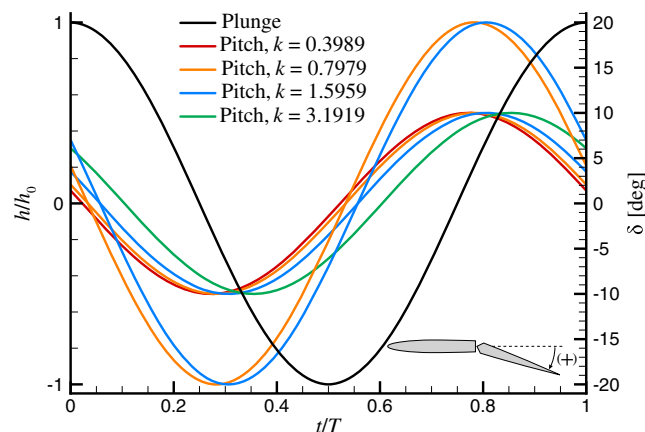


Fig. 2 Combined plunge and flap-pitch maneuver history for various pitch phases and amplitudes considered for Theodorsen's model.

$$y_k = \begin{bmatrix} \tilde{C} & C_{L_\theta} & C_{L_{\dot{\theta}}} \end{bmatrix} \begin{bmatrix} \tilde{x}_k \\ \theta_k \\ \dot{\theta}_k \end{bmatrix} + C_{L_{\ddot{\theta}}} \ddot{\theta}_k \quad (9b)$$

was developed, where prior knowledge of the kinematic relation from $\ddot{\theta}$ to $\{\theta, \dot{\theta}\}$ was leveraged. The internal state of the system $\tilde{x} \in \mathbb{R}^n$ captured transient aerodynamic effects. Following the approach in [18], the equations of motion were written to a form that was conducive to solving for the unknown dynamics using standard parametric system identification methods. Specifically, known kinematic quantities were treated as inputs for the purposes of system identification, i.e., $u_k = (\ddot{\theta}_k, \dot{\theta}_k, \theta_k)$, and worked with the linear time-invariant (LTI) system in the form

$$\tilde{x}_{k+1} = \tilde{A}\tilde{x}_k + \underbrace{\begin{bmatrix} B_{\ddot{\theta}} & B_{\dot{\theta}} & B_\theta \end{bmatrix}}_{\tilde{B}} u_k \quad (10a)$$

$$y_k = \tilde{C}\tilde{x}_k + \underbrace{\begin{bmatrix} C_{L_{\ddot{\theta}}} & C_{L_{\dot{\theta}}} & C_{L_\theta} \end{bmatrix}}_{\tilde{D}} u_k \quad (10b)$$

Given a sequence of empirical input–output training data $\{u_k^{\text{train}}, y_k^{\text{train}}\}$ with $k = 1, \dots, N$, the unknown system matrices are parameterized as $\xi := (\tilde{A}, \tilde{B}, \tilde{C}, \tilde{D})$ and then determined by solving the following optimization:

$$\begin{aligned} \min_{\xi} J(\xi) &:= \sum_{k=1}^N \|y_k^{\text{train}} - y_k(\xi)\|_2^2 \\ \text{subject to } \tilde{x}_{k+1}(\xi) &= \tilde{A}\tilde{x}_k(\xi) + \tilde{B}\tilde{u}_k \\ \tilde{y}_k(\xi) &= \tilde{C}\tilde{x}_k(\xi) + \tilde{D}\tilde{u}_k \end{aligned} \quad (11)$$

where $y_k(\xi)$ denotes the model-predicted output corresponding to the parameter ξ . The nonlinear least-squares problem in Eq. (11) is solved with the Levenberg–Marquardt algorithm [28]. The optimal solution ξ^{opt} is mapped back to the original discrete-time system model in Eq. (3.2), then converted to a continuous-time system realization using a Tustin transformation [29] in order to compare directly with the Theodorsen models of the previous section.

The flap-pitch and wing-plunge models were constructed independently by respective pure-deflection and pure-plunge motions provided by a smoothed ramp fitted to a semiperiod sinusoidal profile of reduced frequency $k = 1.59$, following a C^∞ -smoothing ramp function provided by Ol et al. [30] given in Eq. (12):

$$\delta(t) = \frac{\hat{\kappa}}{a} \ln \left[\frac{\cosh(a(t-t_1)U_\infty/b)}{\cosh(a(t-t_2)U_\infty/b)} \right] + \frac{\Delta\delta}{2} \quad (12)$$

where $\hat{\kappa} = \dot{\delta}_{\text{max}} b / 2U_\infty$ is the nominal pitch (or plunge) rate, $a = \pi^2 \hat{\kappa} / (2|\Delta\delta|(1-\sigma))$ is the smoothing parameter, σ is a fitting parameter proposed by Granlund et al. [31], $\Delta\delta$ is the difference between the final flap position and the initial flap position, and time constants t_1 and t_2 correspond to the start and completion of flap (or plunge) motion for the nonsmoothed ramp profile. Note that Eq. (12) may be applied to plunge by simple substitution of Δh in place of $\Delta\delta$. The resulting profile is plotted in Fig. 3.

As displayed in Fig. 3, the plunge model was constructed from a plunge maneuver of $\Delta h = 0.6$, and the flap-pitch model was constructed from a pitch maneuver of $\Delta\delta = 20^\circ$. The speed of motion amounted to a smoothed step change where motion is completed in one convective time. The flap was deflected from an initial incidence of $\delta = 0^\circ$ and concluded at $\delta = 20^\circ$ in a flap pitch-hold maneuver. The wing was plunged a depth of $h/b = 0.6$. During plunge the wing remains nondeflected. Reconstructed lift histories are compared with guiding experimental measurements in Fig. 4. The dimension of the

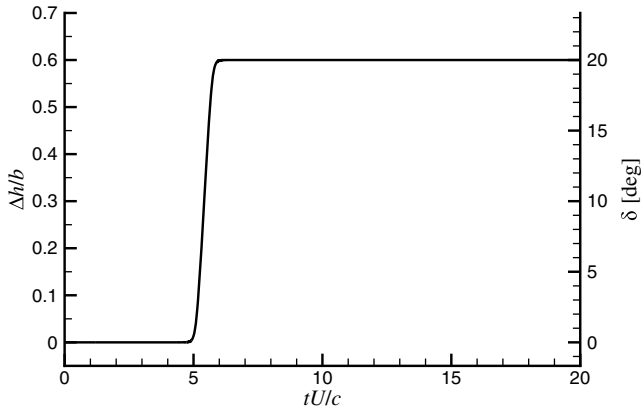


Fig. 3 Smoothed-ramp profile shared among both pure plunge and pure flap-pitch maneuvers.

internal state $\tilde{x}(t)$ was varied from $n = 1$ to $n = 3$. For pure deflection, $n = 1$ was selected to model the lift response, as it had the best qualitative agreement with the initial transient before relaxation.

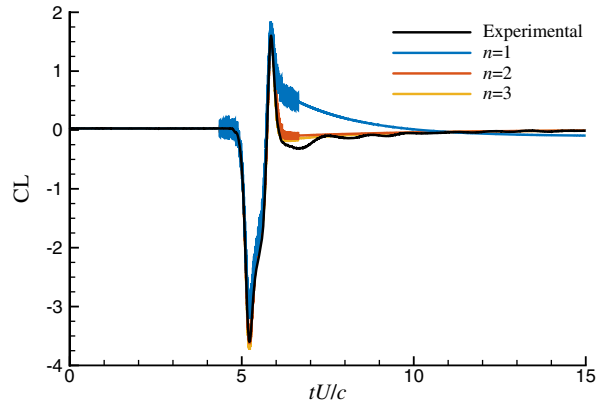
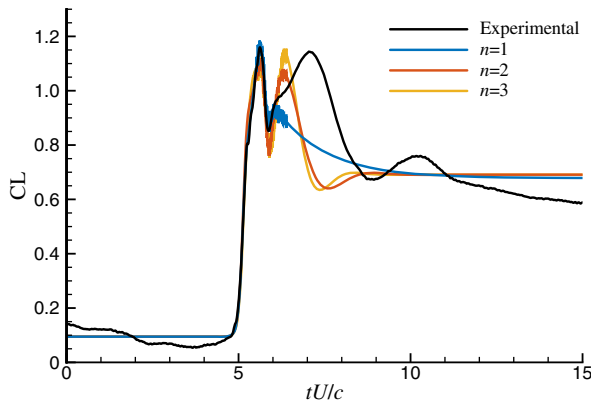


Fig. 4 Indicial response reconstruction: *left*, pure flap deflection; *right*, pure wing plunge.

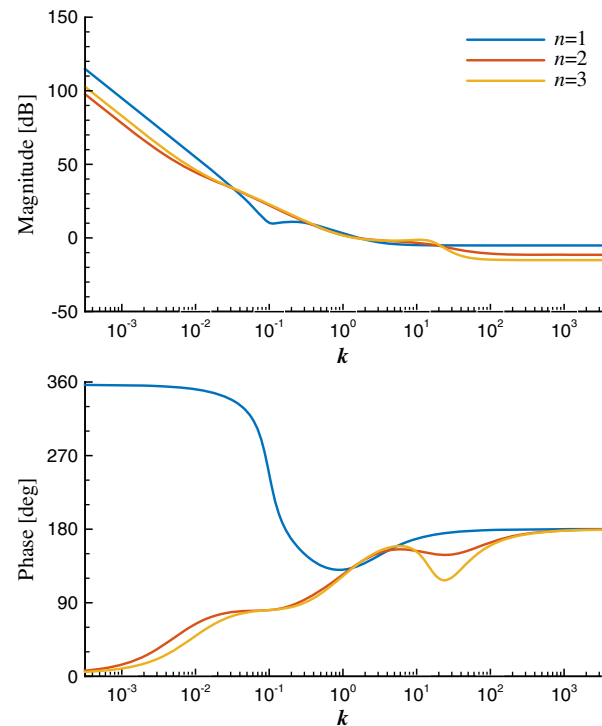
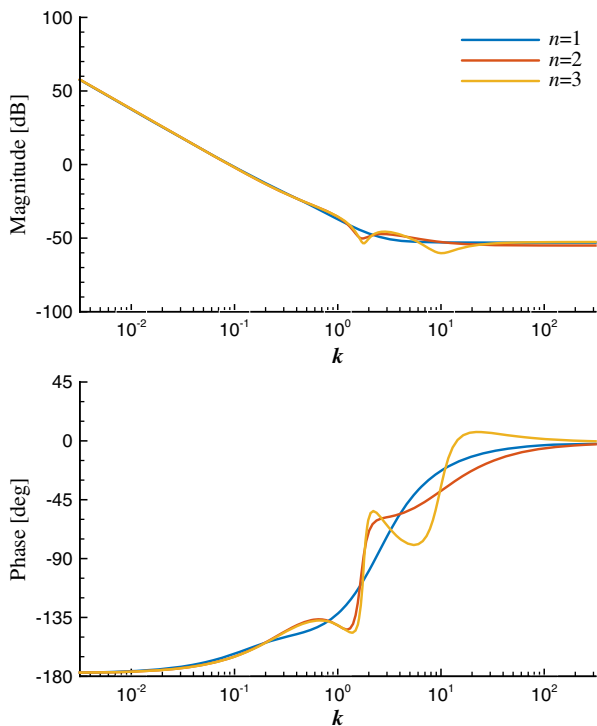


Fig. 5 Frequency response of transfer functions. Columns: *left*, pure flap deflection; *right*, pure wing plunge.

Higher-order models exhibited oscillatory modes. In pure plunge, $n = 2$ was selected to model the lift response, as this was found to capture the force history most accurately.

The frequency responses of the modeled transfer functions for flap deflection, $G_{\text{defl.}}(s) = \mathcal{L}[C_L]/\mathcal{L}[\delta]$, and plunge, $G_{\text{plunge}}(s) = \mathcal{L}[C_L]/\mathcal{L}[\dot{h}]$, are shown in Fig. 5. Here, \mathcal{L} denotes the Laplace transform of the associated signal. The input motion is δ for pure deflection and \dot{h} for pure wing plunge. The output is lift coefficient. The procedure to determine the theoretical deflection amplitude and phase lead required to cancel the lift generated by a given plunge is as follows. Ideally, the lift response of the airfoil would be linearly dependent on flap and plunge motions, allowing for the respective contributions to be superimposed for cancellation, as in Eq. (5). The linear approximation yields an expression for plunge and flap deflection magnitude:

$$\|G_{\text{plunge}}\| \|\dot{h}\| + C_{L_o,\text{plunge}} = \|G_{\text{defl.}}\| \|\delta\| + C_{L_o,\text{defl.}} \quad (13)$$

If flap acceleration is used as an input to the model, the plunge acceleration can be determined as

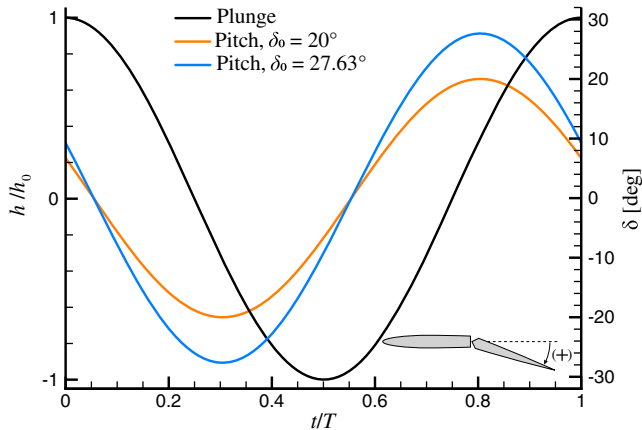


Fig. 6 Combined plunge and flap-pitch maneuver history for various pitch amplitudes at $k = 1.5959$ considered for the empirical model.

$$\|\ddot{h}\| = \frac{(\|G_{\text{defl.}}\| \|\ddot{\delta}\| + C_{L_{\alpha, \text{defl.}}} - C_{L_{\alpha, \text{plunge}}})}{\|G_{\text{plunge}}\|} \quad (14)$$

Alternatively, if plunge acceleration is the input, flap acceleration can be determined using the following expression:

$$\|\ddot{\delta}\| = \frac{(\|G_{\text{plunge}}\| \|\ddot{h}\| + C_{L_{\alpha, \text{plunge}}} - C_{L_{\alpha, \text{defl.}}})}{\|G_{\text{defl.}}\|} \quad (15)$$

The cancellation of lift between airfoil plunging and flap deflection motions requires the lift generated by the two motions to be 180° out of phase with one another. The phase of the lift generated by plunge is equal to the plunge input phase \dot{h} plus the output phase shift in the model, $\angle G_{\text{plunge}}$. A similar relationship exists for flap deflection, yielding the following equation:

$$\angle \dot{h} + \angle G_{\text{plunge}} = \angle \ddot{\delta} + \angle G_{\text{defl.}} + \pi \quad (16)$$

Therefore, the required phase lead ϕ between the airfoil plunge and flap deflection needed to obtain zero lift throughout the motion is determined as

$$\phi = \angle \dot{h} - \angle \ddot{\delta} = \angle G_{\text{defl.}} - \angle G_{\text{plunge}} + \pi \quad (17)$$

where the required phase and magnitude values for a given reduced frequency of operation are populated from the frequency response data of Fig. 5.

Cases that were examined within the state-space framework of the empirical model are summarized in Table 2 and plotted in Fig. 6.

IV. Results and Discussion

Direct force measurements and dye visualization were used to gauge the effectiveness of flap deflection in mitigating the influence of temporal variations in the relative vertical velocity component imposed by airfoil plunge. Before examining the role of dynamic deflection (or plunge) the static lift response is presented to provide

Table 2 Empirical model motion parameters

Case	Motion	h_0/b	ϕ , deg	$\delta(0)$, deg
Case 7: $k = 1.5959$, $\delta_0 = 20^\circ$	Flap+plunge	0.1565	70.41	6.71
	Pure flap	0	180	-20
	Pure plunge	0.1565	0	0
Case 8: $k = 1.5959$, $\delta_0 = 27.63^\circ$	Flap+plunge	0.2057	70.41	9.26
	Pure flap	0	180	-27.63
	Pure plunge	0.2057	0	0

insight into the state of separation experienced over the flap. Results for static lift in response to flap deflection are shown in Fig. 7. As previously noted, the static survey is performed by a slow jog in deflection followed by a hold period. To demonstrate that a steady state is achieved in this approach, static lift was measured for a deflection schedule of $\delta = 0^\circ \rightarrow 20^\circ$, then $20^\circ \rightarrow -20^\circ$, and concluding with $-20^\circ \rightarrow 0^\circ$ with no significant hysteresis observed. Stall is evidenced by the reduction in lift curve slope approaching $\delta = 14^\circ$. By $\delta = 20^\circ$ the flow over the airfoil flap is characterized by its separation envelope spanning the entirety of the flap length, as shown in Fig. 7. A free shear layer is revealed by the dye to be largely streamwise-oriented rather than adhering to the contour of the airfoil flap. The primary focus of the ensuing investigation is a deflection amplitude of $\delta_0 = 20^\circ$. This selection is intended to assess the efficacy of both the theoretical and empirical plunge-mitigation criteria in highly unsteady flows inviting of vortical dynamics.

A. Theoretical Approach: Theodorsen's Model

The theoretical approach to harmonic plunge cancellation follows from enforcing a zero lift criterion of Theodorsen's model. Initial studies examined a deflection amplitude of $\delta_0 = 10^\circ$. As surmised from the static lift slope at $\delta = 10^\circ$ in Fig. 7, this deflection angle presents a nominally attached flow. When engaged in dynamic deflection, the rates of motion considered here are anticipated to support enhanced flow-attachment over the flap [13]. Note that from Eq. (8) the flap deflection phase lead is independent of airfoil plunge or flap deflection amplitudes, consistent with McGowan et al. [23]. However, there is a direct correlation between reduced frequency k and plunge amplitude that may be theoretically canceled. An increase in reduced frequency of flap actuation generates greater periodic lift, which in turn is capable of negating greater plunge-induced lift following more aggressive vertical speeds and accelerations. The acceleration magnitude scales linearly with plunge amplitude and quadratically with reduced frequency. For this reason, reduced frequency values of $k = [0.3989, 0.7979, 1.5959, 3.1919]$ were considered for a flap deflection of $\delta_0 = 10^\circ$. The reduced frequency range targets a highly unsteady flow regime. The corresponding plunge amplitudes and deflection phase leads are summarized in Table 1.

As anticipated, with increasing k there was a decrease in plunge amplitude h/b , although greater noncirculatory forces were generated by the elevated acceleration profile in plunge. This trend is on display in the lift coefficient histories of Fig. 8. Direct force measurements were performed on the airfoil following three kinematic schedules: pure airfoil plunge ($\delta_0 = 0^\circ$), pure flap deflection ($h/b = 0$), and a combined plunge-deflection motion employing the predetermined deflection phase lead. An overarching feature among the pure plunge plots of Fig. 8 is the gradual phase shift of lift coefficient from nominally 90° out of phase from the plunge acceleration of $k = 0.39$ to the gradual synchronization of the lift history with the acceleration profile of $k = 3.19$, in agreement with phase plots of Theodorsen's model [26]. Pure deflection also experiences a gradual shift in lift history phase with increasing reduced frequency k . It should be noted that lift history plots for pure flap deflection are measured from experiment employing zero phase shift

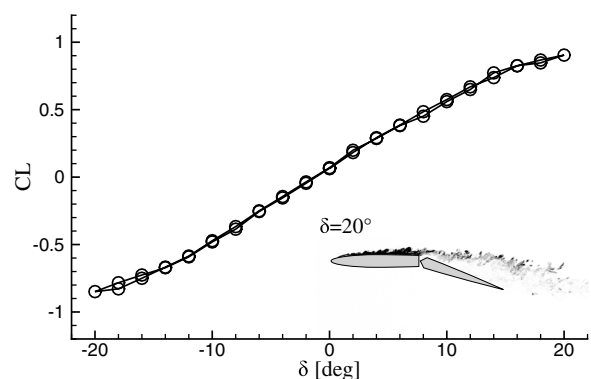


Fig. 7 Static lift coefficient.

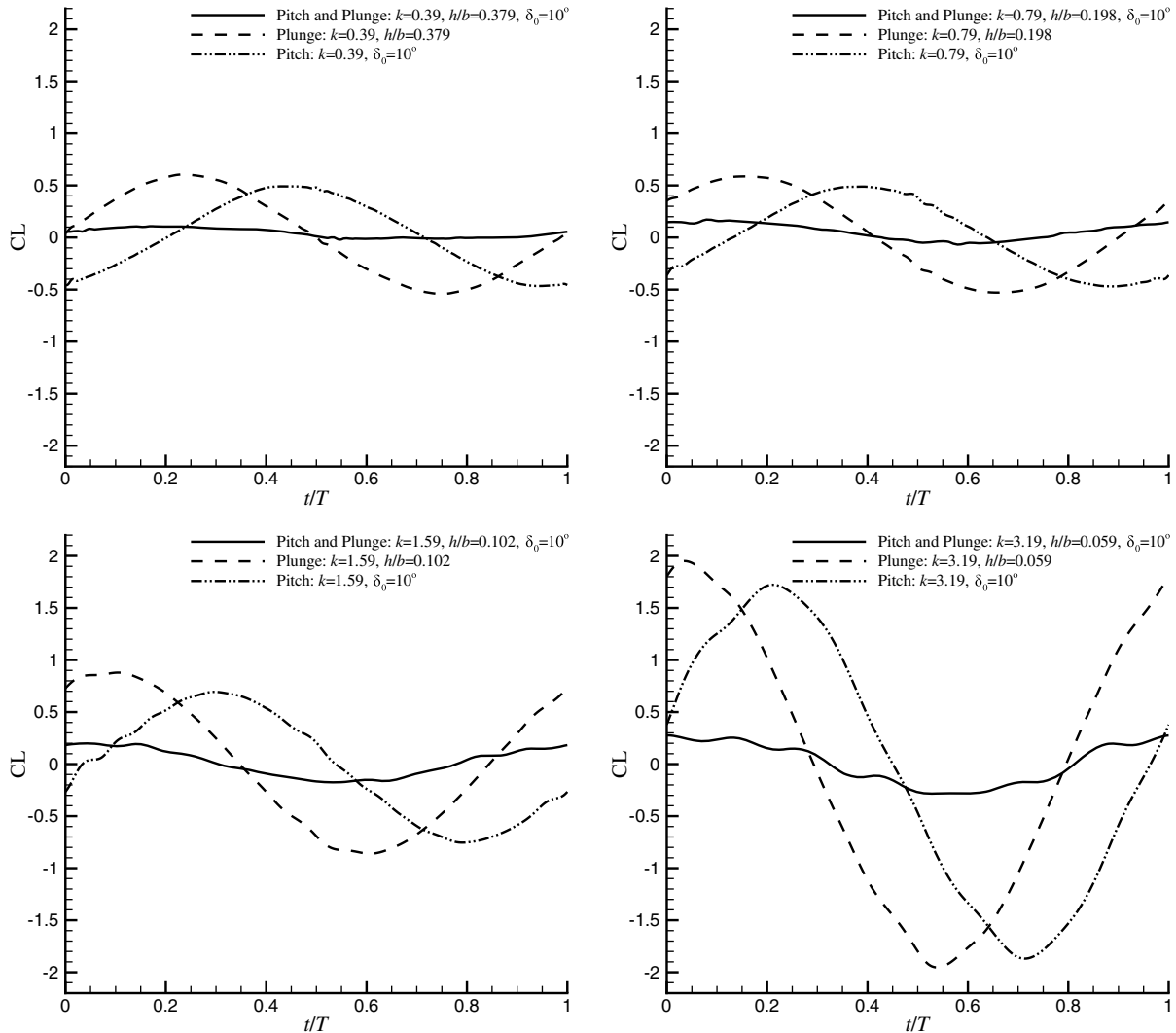


Fig. 8 Theoretical plunge-deflection kinematics: lift history for $\delta_0 = 10^\circ$.

$\phi = 0^\circ$ in Eq. (1). Through application of the Theodorsen’s model, the pure deflection lift histories are of comparable magnitude to those of pure plunge. Pure deflection consistently produces slightly less lift than plunge, and the minor disparity between the two histories’ peak-to-peak lift is nearly doubled from $k = 0.39$ to $k = 3.19$. Nevertheless, when a flap deflection of $\delta_0 = 10^\circ$ was employed in conjunction with the theoretical plunge and phase values, there was a significant drop in lift among the four cases of Fig. 8. There are reductions in lift of 82.2, 74.5, 78.2, and 87.2% from the pure plunge values for reduced frequencies of $k = 0.39, 0.79, 1.59,$ and $3.19,$ respectively. The sizing and kinematic schedule of the flap is successful in enacting significant alleviation of lift generated by harmonic periodic vertical disturbance, congruent with the theoretical zero-lift enforcement of Eq. (5).

When the flap deflection amplitude was increased to $\delta_0 = 20^\circ$, it is expected that a larger plunge excursion could be canceled compared with the previously examined motions at the same reduced frequency for $\delta_0 = 10^\circ$. Lift coefficient histories for $\delta_0 = 20^\circ$ are presented in Fig. 9 for reduced frequencies $k = 0.79$ and 1.59 . For motion at $k = 0.79$, the plunge amplitude theorized for cancellation increased from $h/b = 0.1985$ for $\delta_0 = 10^\circ$ to $h/b = 0.3970$ for $\delta_0 = 20^\circ$. This motion resulted in an 82% reduction in lift from values measured in pure plunge. Likewise, for $k = 1.59$, plunge amplitude was increased to $h/b = 0.2050$, from which pure plunge lift was reduced by 81.4% by flap actuation. There is at present no obvious explanatory trend in cancellation, as at times the reduction in plunge-based lift by flap actuation bore greater success for the higher flap deflection amplitudes than for lower. This observation challenges intuition

concluded from recourse to the small-angle, attached-flow theory of Theodorsen. Intuition is further confounded upon examination of the flow visualizations for $\delta_0 = 20^\circ$.

Figure 10 catalogs the near-body flowfield temporal evolution by way of select snapshots of dye visualization captured throughout a representative kinematic cycle for $k = 0.79$. In the case of pure plunge, leading-edge shear roll-up is prominently represented at $t/T = 0.25$. By $t/T = 0.5$ there is a strong eruption of dye-tagged vorticity emanating from the leading edge to produce a large leading-edge vortex. As the airfoil reciprocates in plunge at $t/T = 0.62$, the parcel of dye, be it the leading-edge vortex or associated free shear layer, is detached and convected along the flap as it is encountered by the airfoil. In this instant, the dye entrained in the leading-edge vortex appears rather dilute given its disbursement over the larger area of the vortex and the influences of diffusion. The leading-edge shear layer on the upper surface of the airfoil ceases to exist, and what remains of the shear layer roll-up is detached from the leading edge and convected downstream. The illuminated surface of the airfoil now acts as the pressure surface and is devoid of vortical formations at $t/T = 0.88$. These unsteady leading-edge formations come as a result of the separation induced by fluctuations in effective angle of attack experienced in plunge. The temporal variation of effective angle of attack is shown in Fig. 12, where it is seen to peak at $\alpha_{\text{eff}} = 17.6^\circ$, well in excess of the stall angle.

Conversely, in pure flap deflection Fig. 10 reveals no vortical aberrations deviating from an otherwise attached flow along the leading edge and the fore element of the airfoil throughout the entire period. The flap deflection amplitude and rate do not appear to induce

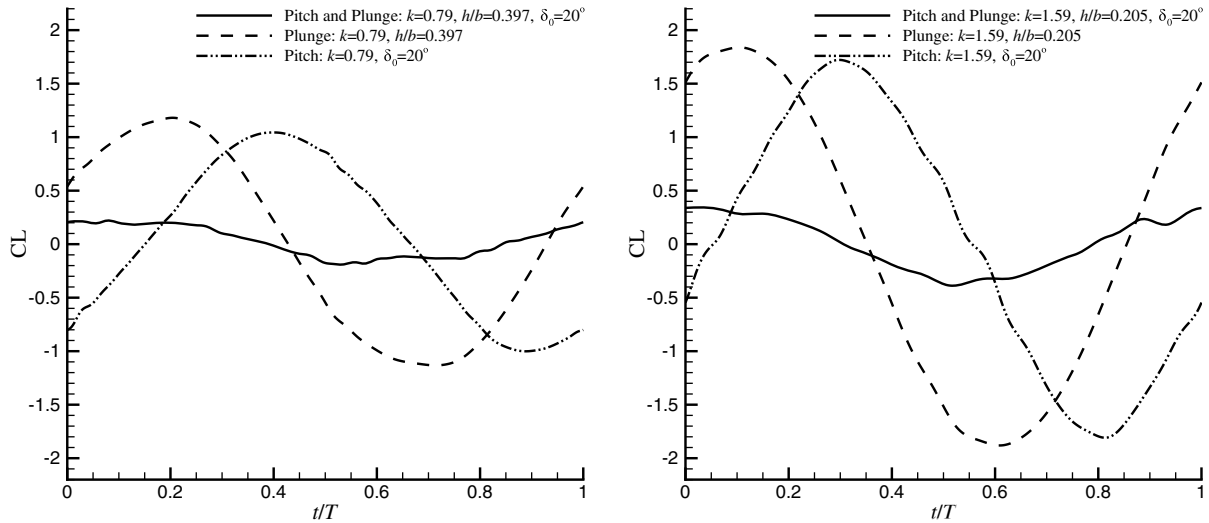


Fig. 9 Theoretical plunge-deflection kinematics: lift history for $\delta_0 = 20^\circ$.

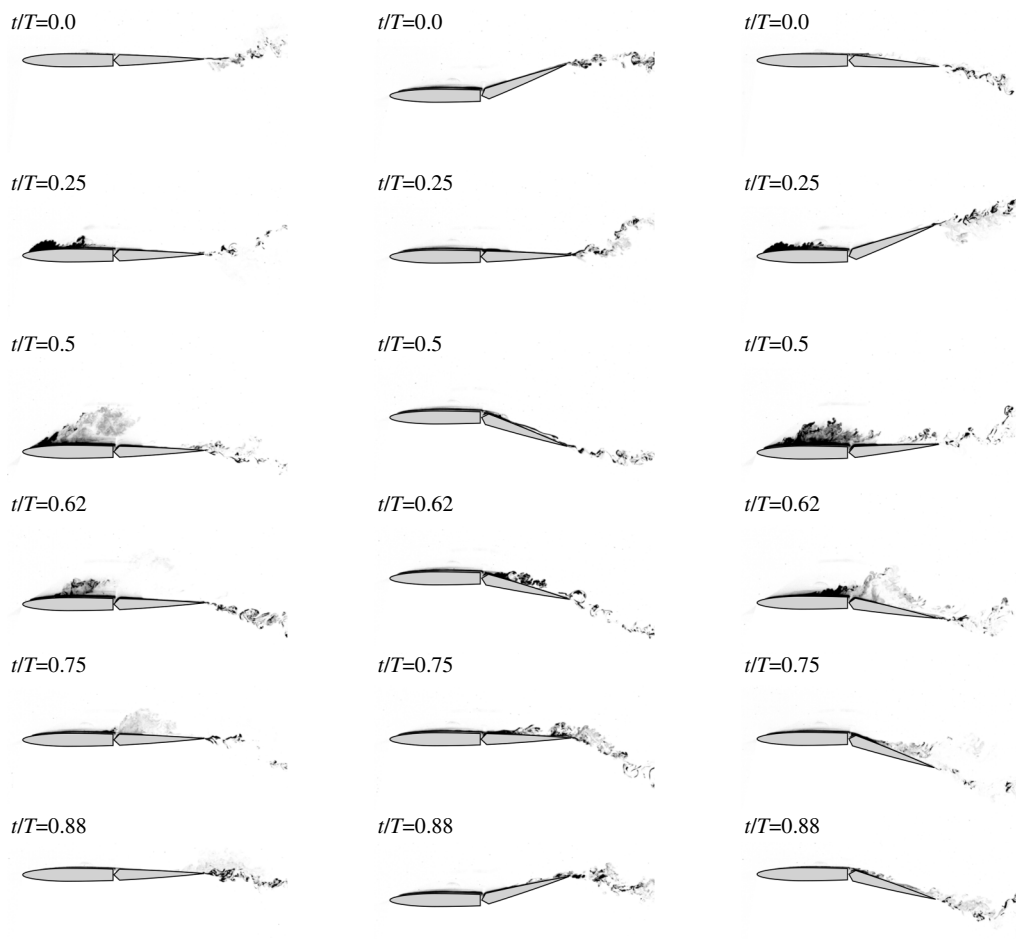


Fig. 10 Theoretical plunge-deflection kinematics: flowfield evolution over one period for $\delta_0 = 20^\circ$ at $k = 0.79$. Columns: *left*, pure plunge; *center*, pure deflection; *right*, plunge and deflection.

leading-edge transient formations. The effects of dynamic deflection appear to be isolated to the near-flap region. As the flap recedes from its maximum deflection at $t/T = 0.62$ the airfoil geometry causes a spurious shear layer mixing over the flap. The resulting formations, however, do not separate from the airfoil, but rather convect along the deflected flap. It would appear then, by inspection of flow visualization, that the onus of flap actuation is both the mitigation of added mass and the suppression of the leading-edge vortex

associated with airfoil plunge. The third column of Fig. 10 shows the plunge-cancellation effects of flap actuation. By as early as $t/T = 0.25$ the flap's effect is discernible by inspection of the shear layer roll-up size, which is reduced from that observed in pure plunge. Perhaps the most telling of leading-edge formation suppression comes at the end of the downstroke at $t/T = 0.5$, where the previous prominence of a leading-edge eruption of vorticity for pure plunge is now subdued in size and distribution for combined plunge

and deflection. That is, the flap motion is not sufficient to provoke the outright cancellation of the leading-edge vortex formation, but it does have substantial influence on its evolution. When the flap is engaged, the leading-edge phenomenon appears more compact and in greater proximity to the airfoil surface. During the upstroke, the flap's deflection also appears to aid in the chordwise convection, and ejection, of vortical formations created in the previous downstroke, as observed at $t/T = 0.75$. Under direct comparison with the pure plunge case it is clear that the dye parcel's convection rate is accelerated in combined plunge and flap pitch. This is in part due to entrainment effects induced by the flap's rapid motion. As the flap is engaged in rapid pitch it draws in the surrounding local flowfield in a direction congruent with the flap's direction of motion. This is the cause for the parcel of dye to be drawn toward the trailing edge at a rate quicker than what is experienced in a nondeflected flap scenario, as is the case in pure plunge. Through these observations, the lift-canceling flowfield does bear many of the hallmarks associated with the pure plunge flowfield, suggesting that the relation between force history and flowfield history is complex.

In doubling the reduced frequency of motion to $k = 1.59$ the general flowfield trend is the development of more coherent and compact structures. Figure 11 catalogs the temporal evolution of the near-body flowfield for $\delta_0 = 20^\circ$, corresponding to the theoretical plunge amplitude of $h/b = 0.205$ at $k = 1.59$ and an effective angle-of-attack peak of $\alpha_{\text{eff}} = 18.2^\circ$ (Fig. 12). For pure airfoil plunge, the semiperiod of motion appears to approach the formation time of the leading-edge vortex. This is ascertained by the airfoil maintaining a concise concentration of vorticity in direct proximity to the leading edge by the completion of the downstroke at $t/T = 0.5$. This introduces an inherent latency in the convection of the leading-edge

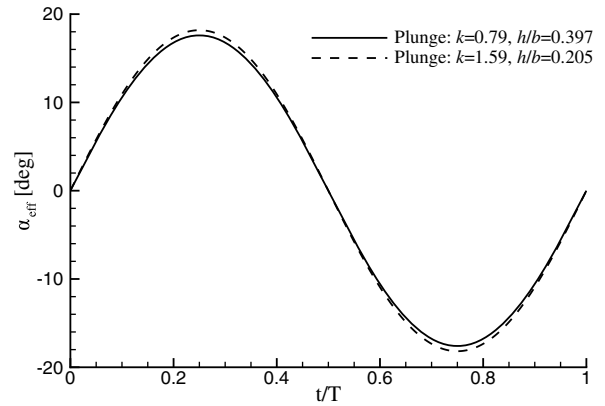


Fig. 12 Effective angle of attack α_{eff} in plunge for theoretically derived kinematics.

formation from that observed for $k = 0.79$, which translates to greater wake interactions during the subsequent upstroke at $t/T = 0.62$. By $t/T = 0.75$ the leading-edge vortex remains a rather prominent feature. Given this structure's prevalence throughout the plunge cycle, it stands to reason that its removal may prove desirable to realize mitigation or cancellation of plunge-based vertical disturbances. As previously observed in pure flap deflection, the leading edge bears no vortical formations induced by trailing-edge flap actuation, as demonstrated in Fig. 11. It is also apparent that flap actuation frequency preserves an attached flow over the flap for the duration of the flap cycle. Minor vortical elements convect along the chord induced by tripping of the boundary layer at the midchord joint.

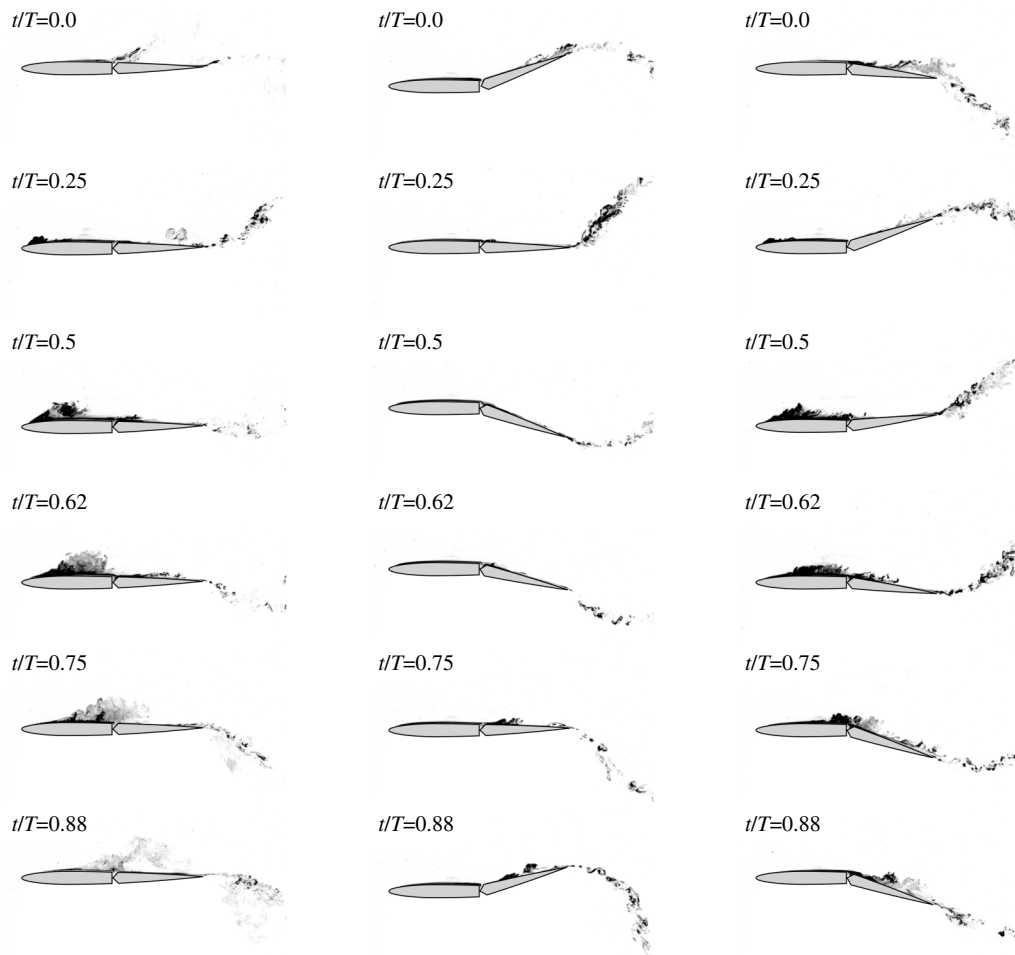


Fig. 11 Theoretical plunge-deflection kinematics: flowfield evolution over one period for $\delta_0 = 20^\circ$ at $k = 1.59$. Columns: *left*, pure plunge; *center*, pure deflection; *right*, plunge and deflection.

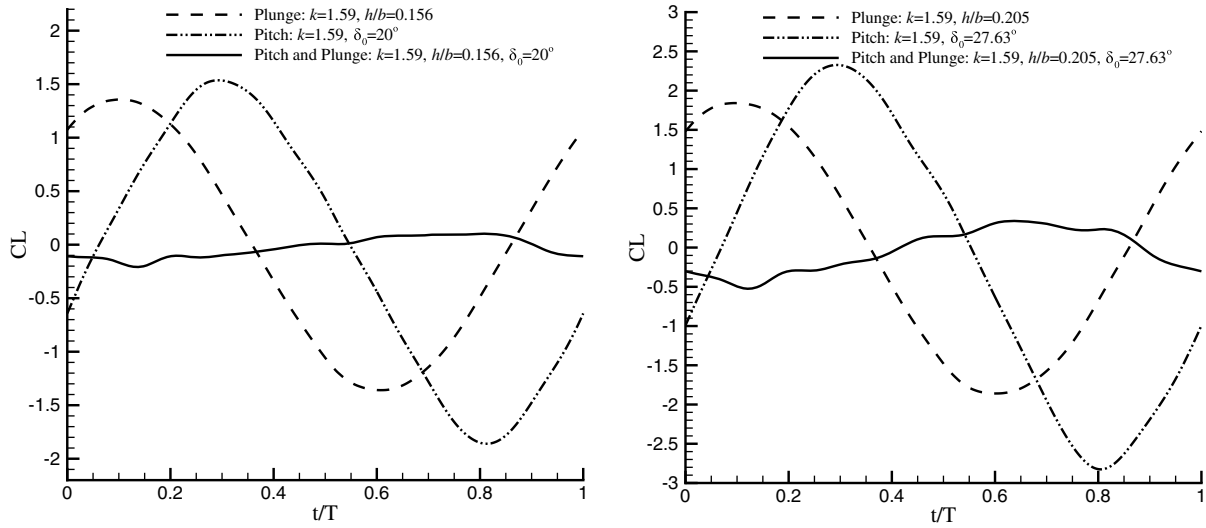


Fig. 13 Empirical plunge-deflection kinematics: lift history for $k = 1.59$.

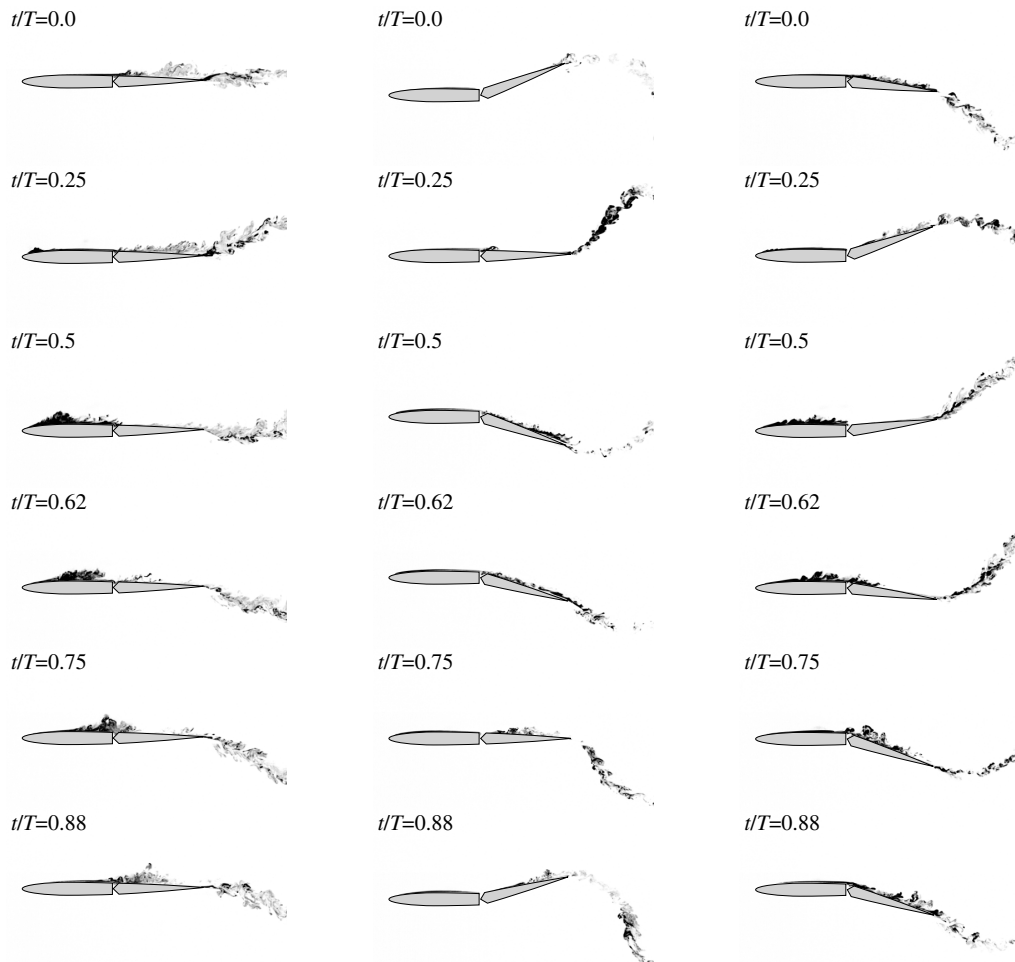


Fig. 14 Empirical plunge-deflection kinematics: flowfield evolution over one period for $\delta_0 = 20^\circ$ at $k = 1.59$. Columns: *left*, pure plunge; *center*, pure deflection; *right*, plunge and deflection.

In combined airfoil plunge and flap deflection, vortical cancellation efforts prove quite effective. At $t/T = 0.5$ it appears that the leading-edge vortex formation has been suppressed, and what remains is the shear-feeding layer. During stroke reversal at $t/T = 0.62$ the wing is left with a semblance of a mixed boundary layer that is spread along the chord. Thus, at $k = 1.59$ the flow remains nominally attached for the entirety of the cancellation cycle.

B. Empirical Approach: State-Space Model

Thus far, Theodorsen's model has been applied to guide kinematic scheduling in plunge-cancellation efforts, and to astonishing success. In an attempt to improve the lift cancellation, a study exploring plunge mitigation via flap actuation with kinematic scheduling determined from empirical modeling of the lift response was explored. The desire here is to improve upon the cancellation efforts of the idealized

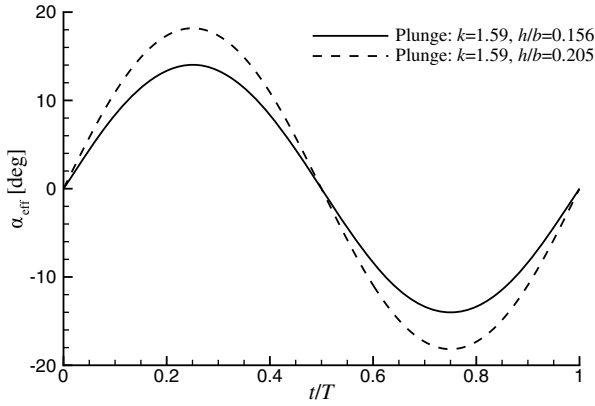


Fig. 15 Effective angle of attack α_{eff} in plunge for empirically derived kinematics.

Theodorsen model. For a flap deflection amplitude of $\delta_0 = 20^\circ$ at $k = 1.59$, Theodorsen’s model indicated a complementary plunge amplitude of $h_0/b = 0.2057$. The resulting lift measurements did leave room for improvement by way of further reducing the lift of combined plunge and deflection closer to zero. Thus it stands to reason that the appropriate plunge amplitude may be smaller than that provided by Theodorsen’s modeling given the lift surplus. To this end, the empirical model reveals a plunge amplitude of $h_0/b = 0.1565$ at $k = 1.59$ with $\delta_0 = 20^\circ$, a 23.9% reduction from Theodorsen’s model. This finding is in qualitative agreement with measured lift trends. The resulting lift histories of the empirically derived kinematics are shown in Fig. 13 (left). In a departure from the

theoretical modeling of Theodorsen, the peak-to-peak lift of pure plunge is now less than that of pure flap deflection. In motions of combined airfoil plunge and flap deflection, once again the resultant lift is significantly reduced from that produced in the pure plunge lift disturbance history. The empirical model boasts a 87.8% reduction from plunge-based lift, an overall improvement over the 81.4% reduction in the lift achieved using the theoretical modeling approach. Congruently, the reduced plunge amplitude of the empirical model is met with further suppression of leading-edge formations, as shown in Fig. 14. Even though the leading-edge roll-up in pure plunge is of smaller-scale given the inherent decrease in plunge velocity due to the fixed reduced frequency, the cancellation efforts of combined plunge and deflection are apparent. Despite the reduction in plunge amplitude, the effective attack angle still manages a substantial peak of $\alpha_{\text{eff}} = 14^\circ$ (Fig. 15). In this instance, much of the plunge-induced formations are relegated to a thin layer of mixing at the end of the downstroke, $t/T = 0.5$, by the flap’s deflection. Beyond the halfstroke, boundary-layer formations are expressly ejected into the wake by the reciprocating deflected airfoil.

As a final case for the empirical model, the plunge amplitude determined from Theodorsen’s model for $\delta_0 = 20^\circ$ at $k = 1.59$ is employed as the input for the empirical model to determine a suitable flap deflection amplitude as output for cancellation. We retain the $h_0/b = 0.2057$ pure-plunge flowfield of Fig. 11 (reproduced in Fig. 16) for its coherent leading-edge vortex, corresponding to a peak in effective attack angle of $\alpha_{\text{eff}} = 18.2^\circ$ (Fig. 15). This case is intended to demonstrate that the gains in disturbance mitigation exhibited by the empirical model for $\delta_0 = 20^\circ$ at $k = 1.59$ are not merely the product of the reduced plunge amplitude but rather speak toward the efficacy of the empirical model. The pitch deflection

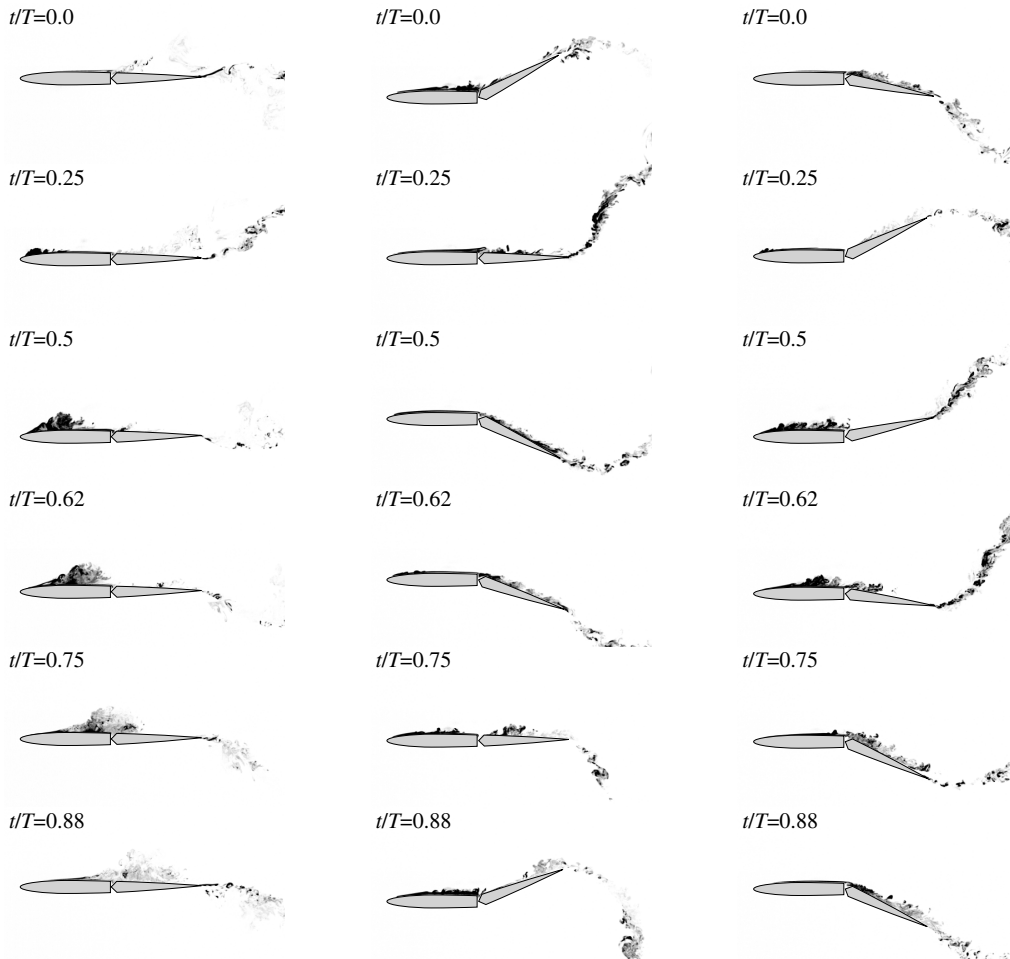


Fig. 16 Empirical plunge-deflection kinematics: flowfield evolution over one period for $\delta_0 = 27.63^\circ$ at $k = 1.59$. Columns: *left*, pure plunge; *center*, pure deflection; *right*, plunge and deflection.

amplitude determined using the empirical model is $\delta_0 = 27.63^\circ$. The corresponding lift histories are presented in Fig. 13 (right). With a phase lead of $\phi = 70.41^\circ$, the dynamics of the flap produce a 81.6% reduction of pure plunge lift. It should be noted that the noncirculatory contribution to peak lift in pure plunge for $k = 1.59$ amounts to 27% of the total lift peak value for both $\delta_0 = 20^\circ$ and 27.63° . Upon examination of the flowfield visualization in Fig. 16 we note that the flowfield remains attached in pure flap deflection motions for the duration of the kinematic cycle despite the greater deflection amplitude. In combined plunge and deflection motions, the resulting flowfield is akin to the findings of the empirical $\delta = 20^\circ$ case in that there is outright suppression of the leading-edge vortex and an express ejection of the mixed boundary layer.

V. Conclusions

A conventional, large (50% chord) trailing-edge flap was deflected in periodic motions with the fore element of the wing held fixed at incidence of $\alpha_{LE} = 0^\circ$ in the presence of an imposed disturbance instantiated as a sinusoidal vertical plunging motion of the entire test article. Flap deflection phase lead and amplitude were derived employing Theodorsen's idealized attached-flow model and empirical models for pure plunge and pure flap deflection treated as a superimposition such that the combined motion of the wing plunge and the flap deflection would give a theoretical net cancellation in lift. Motions derived from Theodorsen's model occurred over a time period of one to eight convective times, the latter approaching a quasi-steady state and the former dominated by added-mass and pitch-rate effects. Although full lift cancellation was not achieved, the theoretical approached yielded substantial mitigation of the plunge disturbance, which in select cases amounted to a residual lift peak of only 13% the pure-plunge lift. Comparisons between the theoretical model and the empirical model were reserved for reduced frequencies $k = 1.59$ and flap deflection amplitudes $\delta_0 \geq 20^\circ$ to invite greater transient vortical formations. Lift histories revealed the performance of the empirical approach to be quite similar to the cancellation efforts of Theodorsen's model. Similarly, the resultant empirical phase leads of flap deflection agree quite well with phase-lead values derived from Theodorsen's model. However, inspection of the accompanying flow visualization reveals greater suppression of the leading-edge vortex generated in pure plunge when employing the empirical models for cancellation.

Acknowledgments

Maziar S. Hemati acknowledges support from the Air Force Office of Scientific Research Grant No. FA9550-19-1-0034. The authors would like to thank Matthew Rockwood for his support on this topic.

References

- [1] Granlund, K., Monnier, B., Ol, M., and Williams, D., "Airfoil Longitudinal Gust Response in Separated vs. Attached Flows," *Physics of Fluids*, Vol. 26, No. 2, 2014, Paper 027103. <https://doi.org/10.1063/1.4864338>
- [2] Choi, J., Colonius, T., and Williams, D. R., "Surging and Plunging Oscillations of an Airfoil at Low Reynolds Number," *Journal of Fluid Mechanics*, Vol. 763, Jan. 2015, pp. 237–253. <https://doi.org/10.1017/jfm.2014.674>
- [3] Dunne, R., and McKeon, B. J., "Dynamic Stall on a Pitching and Surging Airfoil," *Experiments in Fluids*, Vol. 56, No. 8, 2015, pp. 1–15. <https://doi.org/10.1007/s00348-015-2028-1>
- [4] Medina, A., Ol, M. V., Greenblatt, D., Müller-Vahl, H., and Strangfeld, C., "High-Amplitude Surge of a Pitching Airfoil: Complementary Wind- and Water-Tunnel Measurements," *AIAA Journal*, Vol. 56, No. 4, 2018, pp. 1703–1709. <https://doi.org/10.2514/1.J056408>
- [5] Strangfeld, C., Müller-Vahl, H., Nayeri, C. N., Paschereit, C. O., and Greenblatt, D., "Airfoil in a High Amplitude Oscillating Stream," *Journal of Fluid Mechanics*, Vol. 793, April 2016, pp. 79–108. <https://doi.org/10.1017/jfm.2016.126>
- [6] Biler, H., Badrya, C., and Jones, A. R., "Experimental and Computational Investigation of Transverse Gust Encounters," *AIAA Journal*, Vol. 57, No. 11, 2019, pp. 4608–4622. <https://doi.org/10.2514/1.J057646>
- [7] Corkery, S. J., Babinsky, H., and Harvey, J. K., "On the Development and Early Observations from a Towing Tank-Based Transverse Wing-Gust Encounter Test Rig," *Experiments in Fluids*, Vol. 59, No. 135, 2018, pp. 1–16. <https://doi.org/10.1007/s00348-018-2586-0>
- [8] Grubb, A. L., Moushegian, A., Heathcote, D. J., and Smith, M. J., "Physics and Computational Modeling of Nonlinear Transverse Gust Encounters," *AIAA Scitech 2020 Forum*, AIAA Paper 2020-0080, 2020. <https://doi.org/10.2514/6.2020-0080>
- [9] Sedky, G., Jones, A. R., and Lagor, F., "Lift Modeling and Regulation for a Finite Wing During Transverse Gust Encounters," *AIAA Scitech 2019 Forum*, AIAA Paper 2019-1146, 2019. <https://doi.org/10.2514/6.2019-1146>
- [10] Perrotta, G., and Jones, A. R., "Unsteady Forcing on a Flat-Plate Wing in Large Transverse Gusts," *Experiments in Fluids*, Vol. 58, No. 8, 2017, pp. 1–11. <https://doi.org/10.1007/s00348-017-2385-z>
- [11] Mueller-Vahl, H., Strangfeld, C., Nayeri, C., Paschereit, C., and Greenblatt, D., "Dynamic Stall Under Combined Pitching and Surging," *AIAA Journal*, Vol. 58, No. 12, 2020, pp. 5134–5145.
- [12] Rennie, R., and Jumper, E., "Experimental Measurements of Dynamic Control Surface Effectiveness," *Journal of Aircraft*, Vol. 33, No. 5, 1996, pp. 880–887. <https://doi.org/10.2514/3.47030>
- [13] Medina, A., Ol, M., Mancini, P., and Jones, A., "Revisiting Conventional Flaps at High Deflection Rate," *AIAA Journal*, Vol. 55, No. 8, 2017, pp. 2676–2685. <https://doi.org/10.2514/1.J055754>
- [14] Medina, A., Hemati, M., and Rockwood, M., "Separated Flow Response to Rapid Flap Deflection," *AIAA Journal*, Vol. 58, No. 4, 2020, pp. 1446–1457. <https://doi.org/10.2514/1.J058367>
- [15] Brennen, C., "A Review of Added Mass and Fluid Inertial Forces," Naval Civil Engineering Lab. CR 82.010, Port Hueneme, CA, 1982.
- [16] Jaworski, J., "Thrust and Aerodynamic Forces from an Oscillating Leading Edge Flap," *AIAA Journal*, Vol. 50, No. 12, 2012, pp. 2928–2931. <https://doi.org/10.2514/1.J051579>
- [17] Medina, A., Ol, M., Williams, D., An, X., and Hemati, M., "Modeling of Conventional Flaps at High Deflection-Rate," *55th AIAA Aerospace Sciences Meeting*, AIAA Paper 2017-1230, 2017. <https://doi.org/10.2514/6.2017-1230>
- [18] Hemati, M., Dawson, S., and Rowley, C., "Parameter-Varying Aerodynamics Models for Aggressive Pitching-Response Prediction," *AIAA Journal*, Vol. 55, No. 3, 2017, pp. 693–701. <https://doi.org/10.2514/1.J055193>
- [19] Greenblatt, D., and Wagnanski, I., "The Control of Flow Separation by Periodic Excitation," *Progress in Aerospace Sciences*, Vol. 36, No. 7, 2000, pp. 487–545. [https://doi.org/10.1016/S0376-0421\(00\)00008-7](https://doi.org/10.1016/S0376-0421(00)00008-7)
- [20] Rennie, R., and Jumper, E., "A Case for Pseudo-Steady Aerodynamic Behavior at High Motion Rates," *35th Aerospace Sciences Meeting and Exhibit*, AIAA Paper 1997-0617, 1997.
- [21] Albrecht, T., Weier, T., Gerbeth, G., Monnier, B., and Williams, D., "Separated Flow Response to Single Pulse Actuation," *AIAA Journal*, Vol. 53, No. 1, 2015, pp. 190–199. <https://doi.org/10.2514/1.J053026>
- [22] Sedky, G., Jones, A., and Lagor, F., "Lift Modeling and Regulation for a Finite Wing During Transverse Gust Encounters," *AIAA Scitech 2019 Forum*, AIAA Paper 2019-1146, 2019. <https://doi.org/10.2514/6.2019-1146>
- [23] McGowan, G., Granlund, K., Ol, M., Gopalarathnam, A., and Edwards, J., "Investigation of Lift-Based Pitch-Plunge Equivalence for Airfoils at Low Reynolds Numbers," *AIAA Journal*, Vol. 49, No. 7, 2011, pp. 1511–1524. <https://doi.org/10.2514/1.J050924>
- [24] Kerstens, W., Pfeiffer, J., Williams, D., and King, R., "Closed-Loop Control of Lift for Longitudinal Gust Suppression at Low Reynolds Numbers," *AIAA Journal*, Vol. 49, No. 8, 2011, pp. 1721–1728. <https://doi.org/10.2514/1.J050954>
- [25] Medina, A., and Hemati, M., "Lift Disturbance Cancellation with Fast-Flap Actuation," *2018 Fluid Dynamics Conference*, AIAA Paper 2018-3090, 2018. <https://doi.org/10.2514/6.2018-3090>
- [26] Brunton, S. L., and Rowley, C. W., "Empirical State-Space Representations for Theodorsen's Lift Model," *Journal of Fluids and Structures*,

- Vol. 38, April 2013, pp. 174–186.
<https://doi.org/10.1016/j.jfluidstructs.2012.10.005>
- [27] Brunton, S. L., Dawson, S. T. M., and Rowley, C. W., “State-Space Model Identification and Feedback Control of Unsteady Aerodynamic Forces,” *Journal of Fluids and Structures*, Vol. 50, Oct. 2014, pp. 253–270.
<https://doi.org/10.1016/j.jfluidstructs.2014.06.026>
- [28] Nocedal, J., and Wright, S. J., *Numerical Optimization*, 2nd ed., Springer, New York, 2006, Chap. 10.
- [29] Åström, K. J., and Wittenmark, B., *Computer-Controlled Systems: Theory and Design*, Prentice–Hall, Upper Saddle River, NJ, 1997, Chap. 8.
- [30] Ol, M., Eldredge, J., and Wang, C., “High-Amplitude Pitch of a Flat Plate: An Abstraction of Perching and Flapping,” *International Journal of MAVs*, Vol. 1, No. 3, 2009, pp. 203–216.
<https://doi.org/10.1260/175682909789996186>
- [31] Granlund, K. O., Ol, M. V., and Bernal, L. P., “Unsteady Pitching Flat Plates,” *Journal of Fluid Mechanics*, Vol. 733, Oct. 2013, Paper R5.
<https://doi.org/10.1017/jfm.2013.444>

H. Dong
Associate Editor